Fabrication and characterization of hermetic solid oxide fuel cells without sealant

Charles Compson, Meilin Liu *

Georgia Institute of Technology, School of Materials Science and Engineering, 771 Ferst Drive, Atlanta, GA 30332-0245, USA

Abstract

A simplified solid oxide fuel cell (SOFC) design has been developed that would eliminate the need for external sealants yet maintains the hermetic requirements necessary for separation of fuel from oxidant. This hermetic seal is based on the formation of a solid-state interface, between the electrolyte and the interconnect. The novel SOFC design eliminates unnecessary interface formation and material addition, thus greatly simplifying fuel cell stacks. Overcasting and co-casting techniques were used to fabricate symmetric cell and lateral geometries in order to examine the interfacial characteristics of the hermetic structure and particularly the solid-state seal. Leakage rates determined from mass spectrometry were about $4.57*10^{-7}$ L/s at 750 °C.
© 2005 Elsevier B.V. All rights reserved.

1. Introduction

Solid oxide fuel cells have the potential to be one of the leading energy conversion technologies of the future. They have high electrical efficiency, fuel versatility and low emissions compared with other energy conversion systems. One of the major problems facing the advancement of solid oxide fuel cell (SOFC) technology is sealing between cells in a stack [1,2]. Typical glass and ceramic seals can form reactive phases [3–6], leak [7] and/or degrade [4,6] over time, decreasing SOFC performance. While recent work addressing the issue of SOFC sealant materials shows progress, various problems still remain [1,2]. Hard seals such as those achieved using glass sealant materials are rigid and readily prevent gas mixing, but degrade over time due to atmospheric conditions [3,4,6]. Glass seals also have difficulty relaxing to the thermal stresses of cycling and often crack the materials in which they are in contact. Soft or compressive sealant materials such as various mica compositions and ceramic fiber seals have also been examined [8]. These materials tend to have higher leakage rates than the rigid glass materials, but show better thermal cycling characteristics.

Presently there is no universal sealing method and research to improve stack sealing has centered on glass, ceramic and glass–ceramic hybrid materials [10]. Hybrid sealant materials developed at PNNL have achieved leakage rates as low as $1.67*10^{-5}$ L/s/m (0.01 sccm/cm) at 800 °C for polycrystalline muscovite and phlogopite mica layers under $6.89*10^{-5}$–$2.76*10^6$ Pa (100–400 psi) compressive stresses [11]. Hybrid sealants using single crystal muscovite mica show leakage rates two orders of magnitude lower at compressive stresses of $1.72*10^5$–$6.89*10^5$ Pa (25–100 psi), which are some of the lowest reported in literature [11–14].
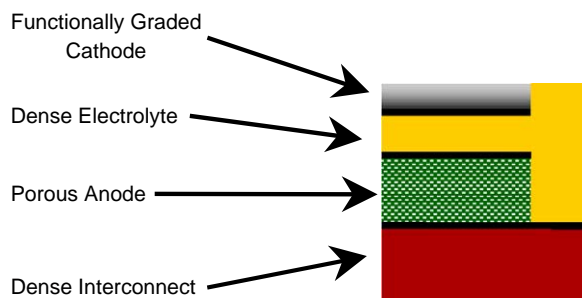

Fig. 1. Novel SOFC design for hermetic seal without sealant [15].

---

* Corresponding author. Tel.: +1 404 894 6114; fax: +1 404 894 9140.
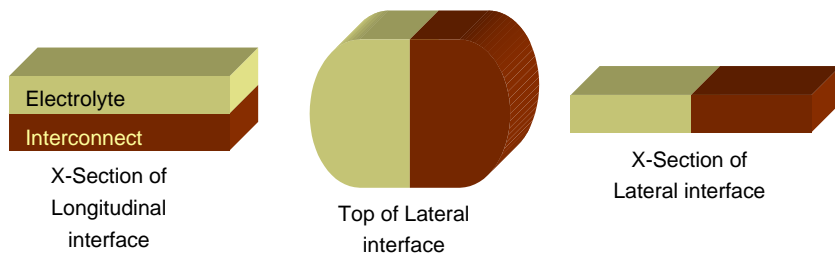 *E-mail address:* Meilin.Liu@mse.gatech.edu (M. Liu).

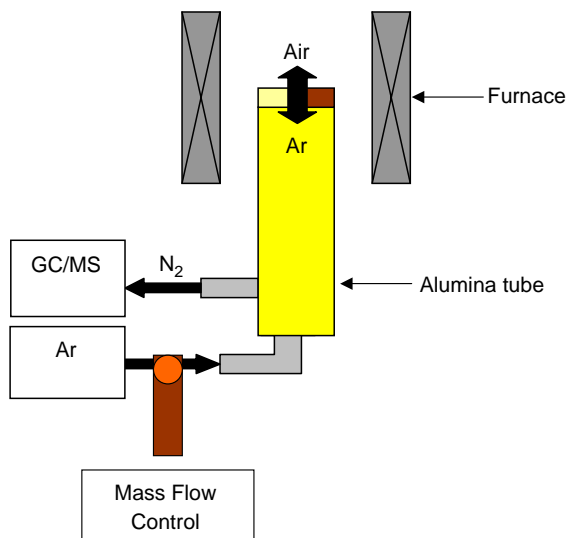Fig. 2. Schematics of longitudinal and lateral interfaces.

Fig. 3. Experimental setup for lateral interface leakage rate testing.

A unique SOFC design has been developed aiming at reducing system complexity by decreasing the number of components and interfaces. The design forms an inherent solid-state seal between interconnect and electrolyte through expansion of the electrolyte layer beyond the anode chamber and down to interconnect. This exploits the requirements of the separator and sealant because both need to be dense, gas impermeable, non-reactive/chemically compatible with surrounding components and atmospheres as well as unaffected by the operating temperature. Since the primary SOFC components need to have similar CTE, the sealing capability of this interface will be determined by its ability to block gas transport and should not be confounded by thermal issues. A schematic of the proposed hermetic design is shown in Fig. 1.
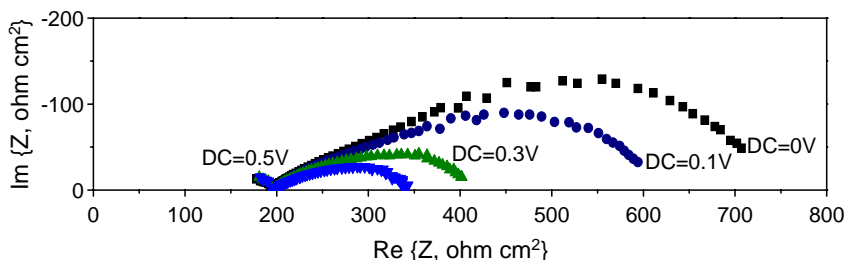
2. Experimental methods

2.1. Sample preparation

To evaluate the sealing capability of the proposed hermetic SOFC structure, the interfacial characteristics of each component in contact with the interconnect were examined. Symmetric cells of anode–interconnect and electrolyte–interconnect were fabricated in order to isolate the desired interface. The electrolyte–interconnect interface was prepared with two different geometries in order to analyze gas transport characteristics both across and along the interface. The two interfacial geometries, longitudinal and lateral, differed with respect to how the electrolyte and interconnect were positioned, as shown in Fig. 2.

Symmetric cells were fabricated by lamination of individual component tapes, overcasting (longitudinal interface), and co-casting (lateral interface). Iron oxide (Fe_2O_3, >99.5%), nickel oxide (NiO, 97%) and chromium oxide (Cr_2O_3, 99%) powders were purchased from Fisher Scientific as the starting materials for the interconnect slurry. YSZ powder (8 mol%, Daiichi Corporation) with a median particle size of 0.26 μm was used for the electrolyte slurry. The as-received NiO particle size ($d < 10$ μm) was initially too large to remain suspended and therefore was ball milled until it had a particle size of less than 3 μm. The Fe_2O_3 and Cr_2O_3 powders were used as received and had particle sizes of less than 5 μm. Stoichiometric mixtures of the interconnect powders were prepared in order to achieve a final composition of $Fe_{47.5}Ni_{47.5}Cr_5$ ($FeNiCr_5$). This composition was chosen based on the recommendation of Church who studied the physical properties of various SOFC interconnect alloys from room temperature to 750 °C and compared them to YSZ (CTE=$10.5*10^{-6}$ °C) [9].

The interconnect slurry was prepared using 21% solids by volume, 60% by volume of solvent (an even mixture of ethanol

Fig. 4. Impedance spectra of $FeNiCr_5|YSZ|FeNiCr_5$ laminated symmetric cell at 650 °C in air as a function of DC bias.

other constituents. Ball-milling was then resumed for another 24 h before casting the slurries at a blade height of 150 μm on a Mistler TTC-1200 tabletop caster [16]. Lamination of individual tapes was used to fabricate symmetric cells between the anode, electrolyte and interconnect materials. The longitudinal geometry was prepared by casting the electrolyte slurry overtop of the interconnect (overcasting) and then laminating two bilayers together into a symmetric cell. Co-casting or the simultaneous (side-by-side) casting of two slurries was used to fabricate the lateral interface geometry. The cast tapes were allowed to dry overnight before 1.9 cm circular samples were punched, laminated together in a uniaxial press and sintered at 1300 °C in 4% H_2 (balance Ar) for 5 h, a schedule determined by dilatometry. A semi-constrained sintering technique, using 11.5 cm × 11.5 cm alumina firing plates and ceramic spacers of known thickness, was employed to ensure that the resulting samples would not warp during sintering.

2.2. Symmetric cell testing

After sintering, silver electrodes were attached to the symmetric cell samples for testing in reducing ($H_2 + 3\%$
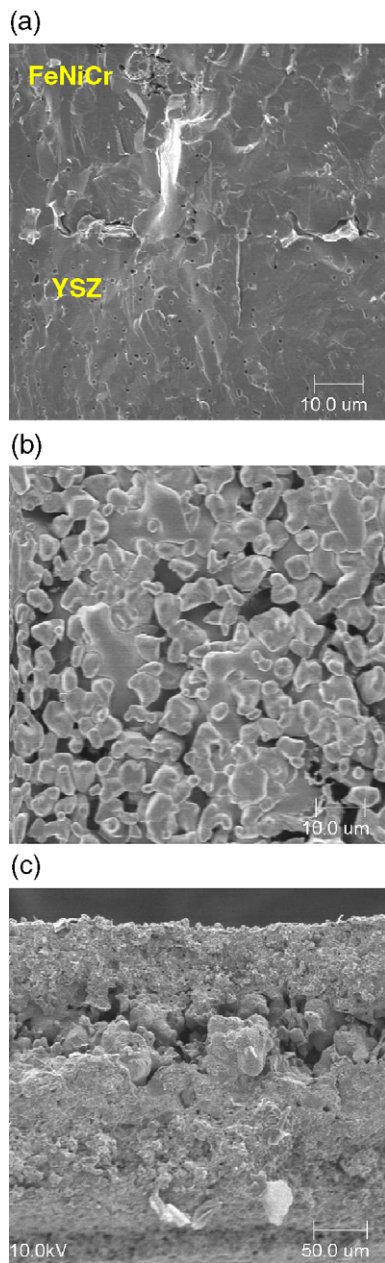
(a)

(b)

(c)

Fig. 5. SEM images of (a) $FeNiCr_5|YSZ$ electrolyte interface before testing, (b) $FeNiCr_5$ surface after testing and (c) $FeNiCr_5$ bulk after testing.

and xylene) and 21% dispersant (Z-3 Menhaden fish oil) with respect to solids content. The remainder of the slurry was organic binder (polyvinyl butyral, B-98) and plasticizer (UCON polyalkylene glycol and S-160 butyl benzyl phthalate) with ratios of 3.8:1 and 2.5:1 to the solids content respectively. The YSZ slurry was prepared using lower solids content (18% by volume) because the median particle size was considerably smaller, 67% by volume of solvent and 21% dispersant with respect to solids content. The same binder and plasticizer organics were added to the slurries in ratios of 3.7:1 and 3:1 of solids content respectively.

All tape cast slurries were prepared using a two-stage milling process. The initial slurry contained only powder, solvent and dispersant and was ball-milled for 4 h prior to addition of the
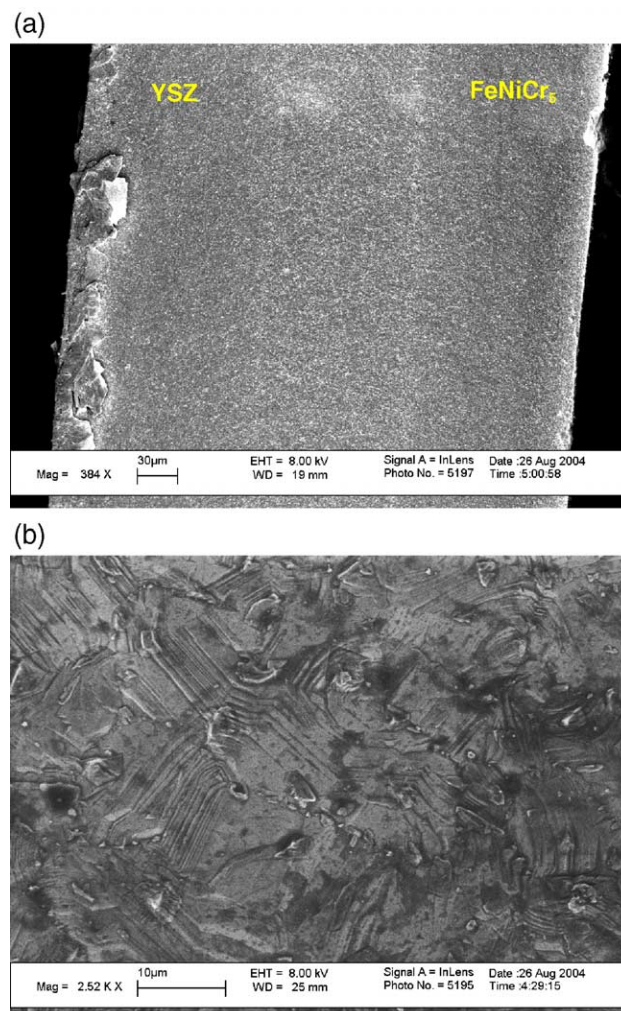
(a)

(b)

Fig. 6. SEM images of (a) $FeNiCr_5|YSZ$ interface by overcasting after testing and (b) dense $FeNiCr_5$ surface after testing.
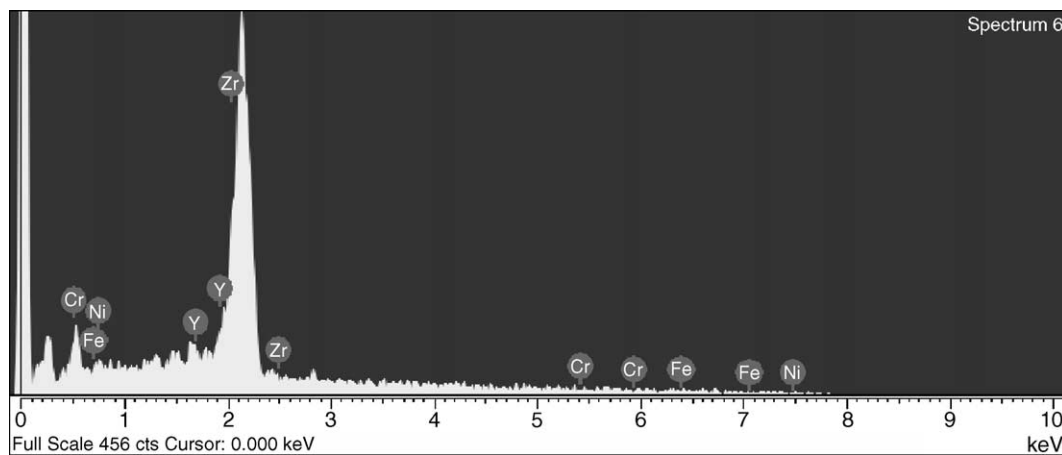
Fig. 7. EDS spectrum of the FeNiCr$_5$|YSZ intermixed region after testing.

H$_2$O), oxidizing (air) and SOFC operating environments. Interfacial properties of the symmetric cells were studied by electrochemical impedance spectroscopy (EIS) as a function of temperature and direct current (DC) bias. Samples were ramped to 550 °C in each atmosphere and held for 30 min before testing. Impedance measurements were conducted in 50 °C increments from 550 °C to 750 °C under open circuit (DC=0 V) and DC bias conditions (DC=0.1, 0.3 and 0.5 V) with 20-min dwell times before each measurement. The frequency was swept from 1 MHz to 20 mHz with an AC perturbation of 20 mV. The above experiments were also repeated for a bulk interconnect pellet of the same composition (Fe$_{47.5}$Ni$_{47.5}$Cr$_5$). This allowed the ohmic contribution of the interconnect to be subtracted from that of the electrolyte in the overall impedance spectra.

2.3. Leakage rate testing

The electrolyte–interconnect lateral geometry samples were sealed to an alumina tube using ceramic cement (Autostic) to determine the leakage rate. The alumina tube setup was mounted in a vertical furnace (ATS clamshell) and manifolded with an inlet gas line with compressed argon flowing through an Omega rotameter. An exit line fed the effluent gas to a mass spectrometer (Hiden Analytical HPR20). The setup for this experiment is shown in Fig. 3.

The furnace was ramped to 550 °C and held for 20 min prior to leakage rate measurement. Argon flow was set to $1.25*10^{-3}$ L/s and the system was held for 10 min to allow for purging of residual water from the gas lines. The partial pressure of oxygen, due to impurity within the argon gas cylinder and gas lines, was also measured to ensure correct determination of oxygen due to seal leakage. Profile scans were taken using the residual gas analyzer with three iterations from 1 amu to 80 amu at 100 samples per atomic mass unit (amu). A Faraday detector collected the signal and the data was reported as pressure intensity versus amu. The leakage rate was determined based on the pressure intensity peak ratios for the detected gases and the assumption of the ideal gas law. Sealing a dense YSZ pellet with the Autostic cement and testing it under identical conditions also determined a baseline leakage rate of the entire setup. This allowed any leakage from the circumference of the pellet–alumina tube interface to be quantified.

3. Results and discussions

3.1. Fabrication of a hermetic interface

The first interfacial geometry, the longitudinal interface, sandwiches the electrolyte in between two interconnect layers in a symmetric cell structure. The longitudinal interface was
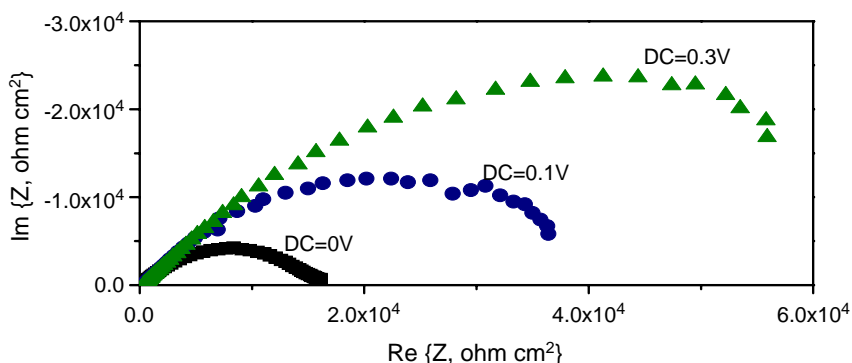

Fig. 8. Impedance of FeNiCr$_5$|YSZ|FeNiCr$_5$ overcast symmetric cell interface at 650 °C as a function of DC bias.
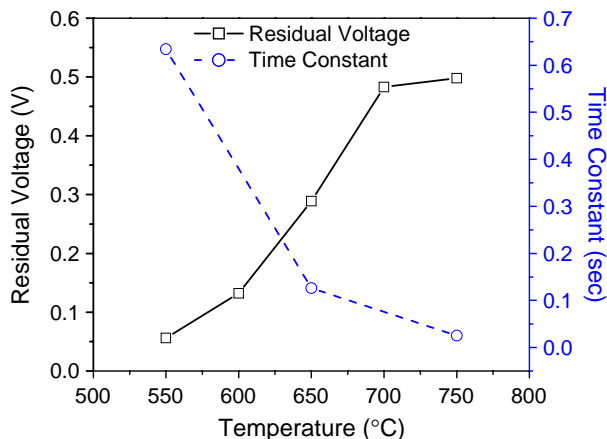
Fig. 9. Residual voltage and relaxation time constant at metal–ceramic interface as a function of temperature.

Fig. 11. Conductivity of NiYSZ|FeNiCr$_5$|NiYSZ symmetric cell in humidified hydrogen.

prepared in order to determine the interfacial characteristics of gas species moving between interconnect and electrolyte layers. Ideally a dense interface forms between the electrolyte and interconnect, which blocks gas transport. Impedance spectroscopy was used to measure the interfacial characteristics as a function of temperature and DC bias, as described above. If gaseous species are being blocked at the electrolyte–interconnect interface, mass transport limitation will result in an increase in impedance with applied DC bias. Blocking gas transport within the cell will also lead to a build up of ions at the interface causing a residual voltage to be retained within the cell even after removal of the applied bias. The ability of the cell to relax or dissipate this charge (relaxation time constant) should be proportional to the porosity of the interface.

Initially symmetric cell samples were prepared by laminating individual layers of interconnect and electrolyte tape together in the uniaxial press. Impedance characterization of the laminated symmetric cell is shown in Fig. 4.

The impedance of the symmetric cell formed by lamination decreased with increased applied DC bias as discussed previously [17]. The decrease in impedance with DC bias was due to the formation of bulk and interfacial porosity during testing. This can be seen in the SEM images, shown in Fig. 5(a–c), of the electrolyte–interconnect interface, interconnect surface and interconnect bulk before and after testing.

Based on the isothermal impedance trend as a function of DC bias it was determined that the sharp interface resulting from lamination of individual electrolyte and interconnect component
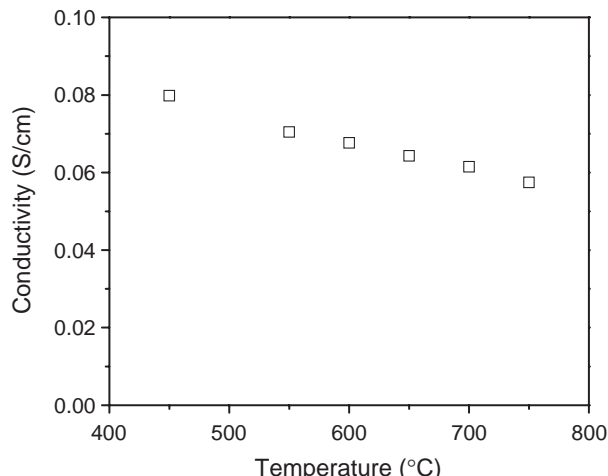
tapes could not form an interface that blocked gas transport. The after-testing SEM images of the interconnect also showed that increased density was necessary. In order to achieve an interface that effectively blocked oxygen transport a fabrication method that allowed a more intimate mixture of the interconnect and electrolyte was required. Intermixing of the two layers was accomplished by overcasting of the electrolyte and interconnect tapes. Instead of casting each layer individually and uniaxially laminating them together, the layers were cast on top of each other while in the green state. The result is shown in Fig. 6, which reveals a large region of intermixing between the YSZ electrolyte and the FeNiCr$_5$ interconnect as well as elimination of interfacial porosity. Another improvement was the surface of the FeNiCr$_5$ material, which shows a dense surface as opposed to the porous surface shown previously in Fig. 4b.

Overcasting fabrication resulted in an intermixed region over 50 μm thick between interconnect and electrolyte layers. Energy dispersive X-ray analysis (EDS) of the intermixed region revealed that it was in fact an intermixture of interconnect and electrolyte materials. The EDS spectrum of the intermixed region is shown below in Fig. 7.

3.2. Impedance analysis of symmetric cell

Electrochemical impedance spectroscopy analysis of the overcast structure in air revealed that the interface formed by overcasting prohibited gas transport. The interfacial resistance
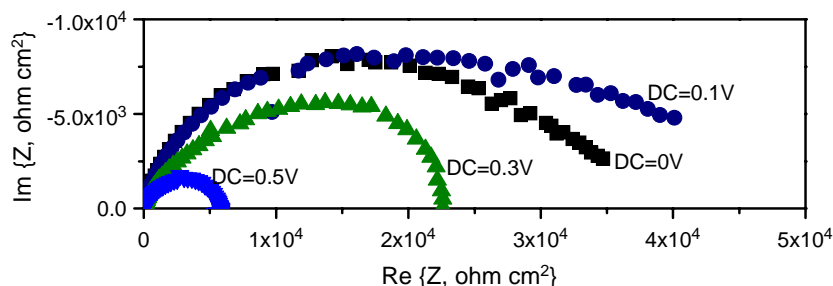
Fig. 10. Impedance spectra of FeNiCr$_5$|YSZ|FeNiCr$_5$ as a function of DC bias in humidified hydrogen at 650 °C.

decreased as a function of temperature in an air atmosphere when not under polarization. Isothermally however, the interfacial impedance increased as a function of DC bias, as seen in Fig. 8, indicating that oxygen ions were blocked at the interface.

After the applied DC bias was removed from the cell, a significant amount of residual voltage remained at the interface. The remnant voltage was a function of both the applied bias and the temperature at which the measurement was taken. At its peak, a residual voltage of 0.498 V remained at the interface after removal of 0.5 V applied bias at 750 °C. Attempts to dissipate the residual charge by shorting the lead wires or just allowing the cell to relax had a negligible effect, implying that the interface formed by overcasting blocks ion transport and stores the charge at the interface. Since the measured relaxation time is slow, on the order of a capacitor, the interface must be dense. These were all desired characteristics for the proposed hermetic SOFC. A plot of the residual voltage at the interface and corresponding relaxation time constant as a function of temperature is shown in Fig. 9.

When the atmosphere was changed to humidified (3 vol.% H_2O) hydrogen, the impedance also decreased as a function of temperature. The desired isothermal impedance trend under DC bias was for the impedance to decrease, which is opposite the trend for the air atmosphere. The proposed structure has one point where the electrolyte–interconnect interface comes in contact with a reducing atmosphere, as seen in Fig. 1, corresponding to a line in three dimensions. Since the electrolyte and interconnect materials are not proton conductors, hydrogen should remain only in the anode chamber during SOFC operation. A decreasing trend in impedance with DC bias corresponds to oxygen ions being pumped into the anode chamber, from within the electrolyte, at a faster rate than under open circuit conditions. These oxygen ions are able to enter the anode both at the top as well as the sides due to the unique higher surface area interface created with the proposed
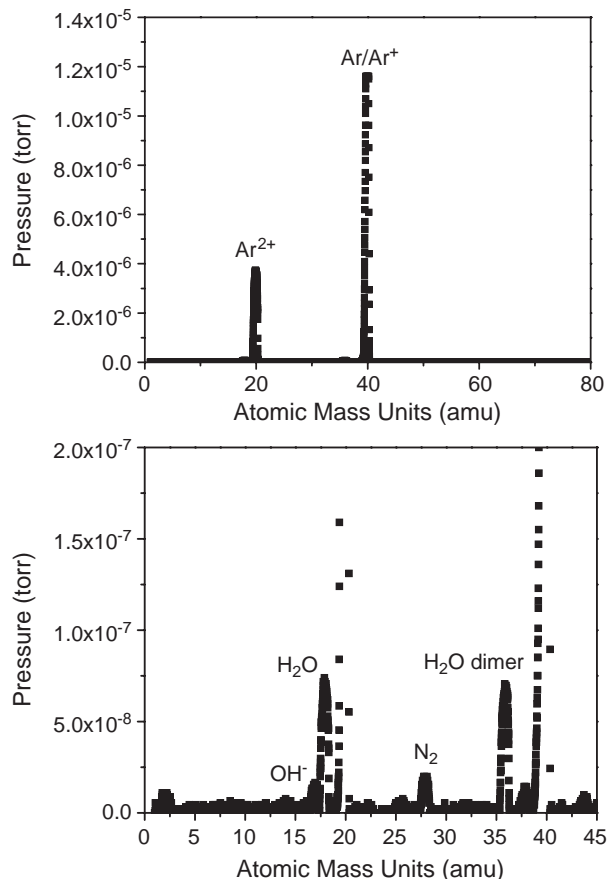

Fig. 13. Mass spectrum from leakage rate testing at 750 °C.

geometry. Therefore the decreasing trend in impedance is acceptable and is shown in Fig. 10.

Oxidation resistance of the interconnect alloy within the symmetric cell was not explicitly measured; however the physical properties and oxidation resistance of this alloy were previously quantified by Church [9]. Church measured the
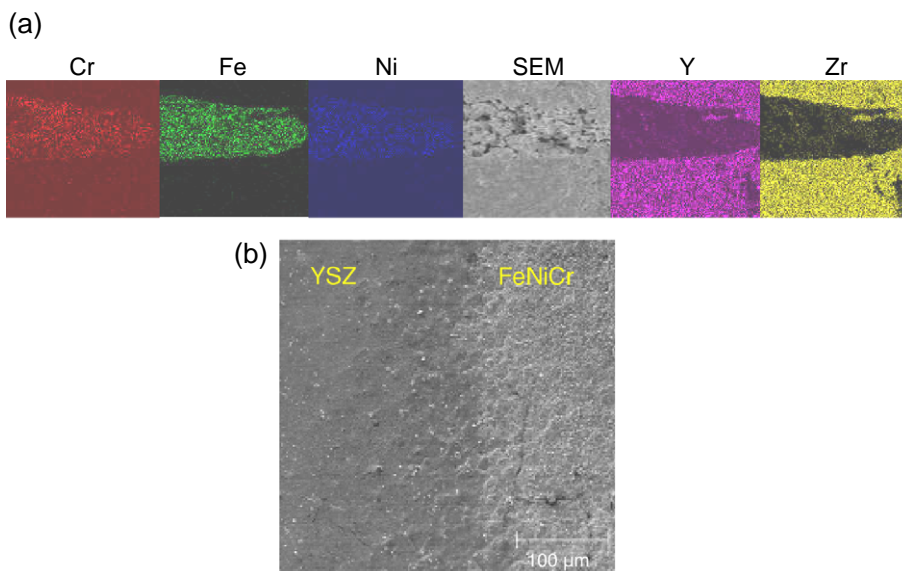

Fig. 12. (a) SEM and EDS dot map of a single YSZ|FeNiCr₅ co-cast layer cross-section and (b) SEM of FeNiCr₅|YSZ surface interface.

Table 1
Leakage rate data as a function of temperature

Temperature (°C)	N_2/O_2 ratio	Leakage rate (L/s)
550	3.696	2.32e − 06
600	3.964	2.22e − 06
650	3.615	1.53e − 06
700	3.545	1.34e − 06
750	3.674	4.42e − 07

Table 2
Leakage rate data as a function of time for isothermal soak at 750 °C

Temperature at 750 °C (s)	N_2/O_2 ratio	Leakage rate (L/s)
600	3.674	3.95e − 07
1800	3.351	6.11e − 07
3600	3.209	6.80e − 07
5400	3.424	7.12e − 07
7200	3.290	8.36e − 07

CTE of the alloy from room temperature to 750 °C and found it to be $9.17 * 10^{-6}$ K^{-1}, which closely mirrored that of YSZ at temperatures above 400 °C. The alloy was also subjected to oxidizing atmosphere at 700 °C for 23 h without significant observation of oxidation, dusting or spalling. The alloy was observed to remain conductive after all symmetric cell measurements up to 750 °C in air and SEM did not reveal any evidence of surface microstructural changes due to oxidation. Switching from an air atmosphere to a hydrogen-containing atmosphere did not appear to affect the sample macrostructure (flatness, shape) or microstructure (cracking due to oxidation–reduction cycling), which also indicates that the interconnect alloy must have entered the hydrogen atmosphere with negligible oxidation.

Symmetric cells involving the anode (NiYSZ) and interconnect were also characterized by impedance spectroscopy. Since the anode and interconnect components would be in contact within the proposed hermetic structure as with any SOFC, the interfacial characteristics needed to be determined. The only atmosphere in which the symmetric cell was tested was humidified hydrogen as that is the only environment this interface will encounter in an SOFC. As would be expected for a cell with a continuous metallic phase, the bulk impedance increased steadily with temperature. Shown in Fig. 11 are the total conductivities of the interconnect–anode symmetric cell, as determined from impedance spectroscopy.

3.3. Leakage rate testing

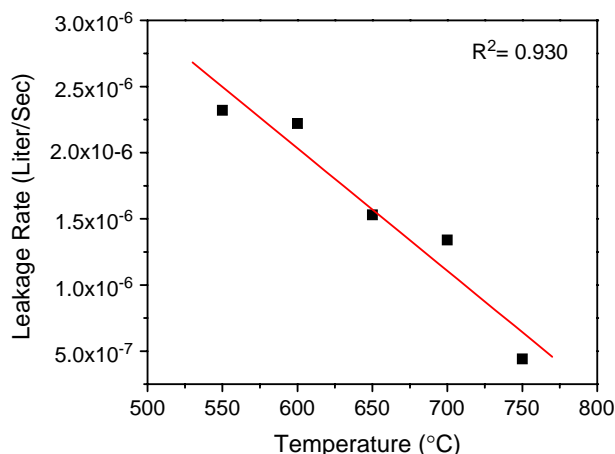The longitudinal geometry samples characterized the gas transport properties across the interface, but not laterally along the interface. Oxygen ions were blocked at the hermetic interface and hydrogen ions kept in the anode chamber, however gas transport from outside the cell into the anode chamber was not determined. Testing the leakage rate of the hermetic structure required preparation of a different interfacial geometry. The type of interface formed within the symmetric cell did not allow for easy cross-sectional manifolding and therefore co-casting method was employed. With this technique the YSZ and interconnect slurries were co-cast into a single tape. After sintering, SEM imaging and EDS dot mapping were conducted on a single layer cross-section, which are shown in Fig. 12(a) and (b).

The interface was not vertical as might be imagined when viewing the top surface, but rather has a more tortuous shape. The formation of a non-linear interface was due to the different shear rate or rheological characteristics of the two slurries. Though both slurries exhibit shear-thinning behavior, they do not have the same shear rate values and thus cast differently. Since the interconnect slurry was less viscous at the shear rate of casting, it cast in a higher surface area geometry than the more viscous YSZ slurry. Three of these layers were aligned, laminated together and sintered to form a cell for leakage rate testing.

The leakage rate of the hermetic SOFC interface was determined using mass spectrometry (as shown in Fig. 3). Lateral interface leakage rates were determined by flowing argon gas through the inlet line and allowing the other side to be exposed to air. The effluent gas was fed to a mass spectrometer for composition determination. Primarily the effluent was probed for the presence of air species (primarily N_2 and O_2), which would correlate to leakage through the

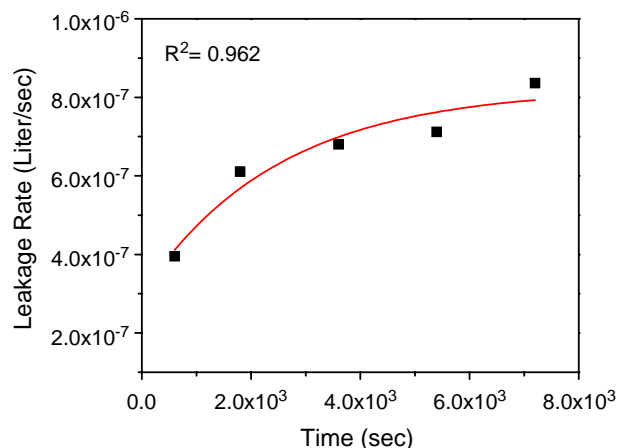Fig. 14. Plot of leakage rate as a function of temperature.

Fig. 15. Plot of leakage rate as a function of time for isothermal soak at 750 °C.
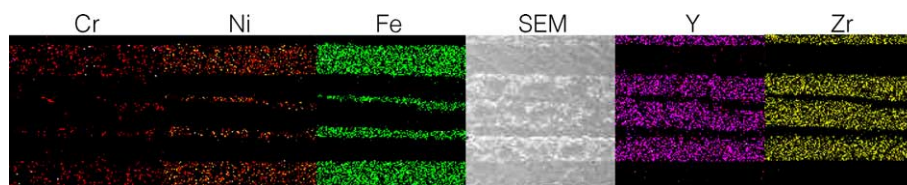
Fig. 16. SEM with EDS dot map of FeNiCr$_5$|YSZ sample used for leakage rate testing.

interface. The amount of oxygen species present within the argon gas cylinder was stated by Air Products to be less than 0.0005%. Due to the inevitable presence of water and trace gas species within the gas lines, the partial pressure of oxygen was measured at the gas outlet in order to be certain the quantified oxygen due to leakage was not being diluted with species from the gas lines. The partial pressure of oxygen was determined to be $1.31 * 10^{-2}$ Pa, which is about 0.0005% of the argon stream. Fig. 13 below is the mass spectrum for the first scan at 750 °C. The top spectrum is the full scale output from the first scan and the bottom spectrum shows a zoomed-in version highlighting the smaller intensity peaks.

Assuming the ideal gas law, the peak intensity ratios were used along with the argon flow rate to determine the leakage rate through the YSZ–FeNiCr$_5$ interface. The resulting leakage rate as a function of temperature is shown in Table 1 and the corresponding trend is plotted in Fig. 14.

The leakage rate as shown in Fig. 14, decreases linearly with increased temperature. The reduction in leakage rate was initially believed to be due to interconnect oxidation and removal of oxygen species from the effluent. This was not the case however, as the nitrogen to oxygen ratio in the effluent remained consistent with that of air and did not show a trend with temperature. The leakage rate decrease is therefore believed to simply be a thermal effect due to increased energy, lattice vibrations and collisions between gas molecules. This increases the tortuosity of the gas molecule path and reduces the leakage rate.

The sample was also held at 750 °C for 2 h, with measurements every 30 m, in order to determine whether the leakage rate changed as a function of time. The leakage rate as a function of time for an isothermal soak at 750 °C is shown in Table 2 and plotted in Fig. 15.

Fig. 15 exhibits a logarithmic trend in leakage rate with time and appears to approach an asymptotic value. Since energy is no longer being increased, the gas transport along the interface can reach steady state, thus establishing equilibrium between the partial pressures of the gas species. This could reasonably be considered the steady state leakage rate for the hermetic seal
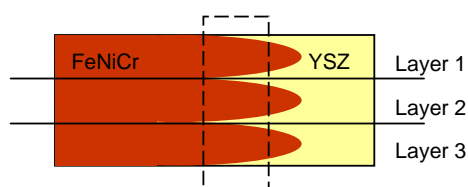
at an operating temperature of 750 °C, given a stationary application.

After testing, the sample was cross-sectioned and again SEM and EDS dot mapping were performed, as seen below in Fig. 16. Since three individual co-cast layers were laminated together to form a single cell, as previously discussed, there is a repeating pattern of Fig. 13(a) within the tested cell.

This cross-section corresponds to the schematic shown in Fig. 17, where the dotted line corresponds to the region being shown in the SEM and EDS dot map and the solid lines represent the individual layers.

Despite the current lack of full cell performance data, it is believed that this solid-state interface has shown the capabilities to adequately seal an SOFC. Future endeavors will concentrate on fabrication of full cells by the tape casting method and also employ other ceramic processing techniques such as screen-printing and electrophoretic deposition. Fabrication will be based primarily on tape casting but may employ other techniques such as screen-printing and electrophoretic deposition to fabricate the desired structure. Dilatometry experiments will be used to identify a firing schedule that accommodates the shrinkage behavior of the fabricated layers such that a single firing step can be used. Performance evaluation of single cells with the critical hermetic seal will ensue and success will be determined based on whether voltages near the theoretical Nernst potential (E_N=1.13 V) can be achieved.

4. Conclusion

Fabrication and characterization of a YSZ–FeNiCr$_5$ interface fabricated by overcasting has shown the ability to block gas transport. Impedance spectroscopy of this interface revealed that as DC bias was increased, the resistance to gas transport increased, indicating that this interface may be able to be used as a seal for SOFCs. Another indication of the quality of the seal was the accumulation of 0.498 V charge at the FeNiCr$_5$–YSZ interface and the presence of a large relaxation time constant. Symmetric cells of NiYSZ and FeNiCr$_5$ yielded the expected trend of low impedance values and therefore would not cause a detriment to the proposed hermetic structure. Leakage rate testing of the hermetic interface showed a decreasing trend in leakage rate with temperature. The leakage rate of the YSZ–FeNiCr$_5$ interface at 750 °C was $4.5 * 10^{-7}$ L/s, which is comparable to the hybrid seal developed at PNNL using polycrystalline mica and glass, which had a leakage rate of $1.67 * 10^{-5}$ L/s/m at 800 °C with $1.72 * 10^5$ Pa compressive stress. Isothermal leakage rates as a function of time did show an increasing logarithmic trend, however the leakage rate appeared to approach an asymptotic value of $8.3 * 10^{-7}$ L/s after 2 h.

Fig. 17. Schematic of FeNiCr$_5$|YSZ lateral interface cross-section showing three laminated co-cast layers.

References

[1] K.S. Weil, C.A. Coyle, J.S. Hardy, J.Y. Kim, G.-G. Xia, Fuel Cells Bull. ((2004) May) 11.
[2] Y.-K. Lee, J.-W. Park, Mater. Chem. Phys. 45 (1996) 97.
[3] N. Lahl, D. Bahadur, L. Singheiser, K. Hilpert, J. Electrochem. Soc. 149 (2002) A607.
[4] Z. Yang, J.W. Stevenson, K.D. Meinhardt, Solid State Ionics 160 (2003) 213.
[5] R. Zheng, S.R. Wang, H.W. Nie, T.-L. Wen, J. Power Sources 128 (2004) 165.
[6] S.-B. Sohn, S.-Y. Choi, G.-H. Kim, H.-S. Song, G.-D. Kim, J. Non-Cryst. Solids 297 (2002) 103.
[7] Y.-S. Chou, J.W. Stevenson, J. Power Sources 112 (2002) 376.
[8] S. Taniguchi, M. Kadowaki, T. Yasuo, Y. Akiyama, Y. Miyake, K. Nishio, J. Power Sources 90 (2000) 163.
[9] B.C. Church, Ph.D. Thesis. Georgia Institute of Technology November (2004).
[10] K.S. Weil, J.Y. Kim, J.S. Hardy, Electrochem. Solid-State Lett. 8 (2005) A133.
[11] Y.-S. Chou, J.W. Stevenson, L.A. Chick, J. Power Sources 112 (2002) 130.
[12] Y.-S. Chou, J.W. Stevenson, J. Power Sources 124 (2003) 473.
[13] Y.-S. Chou, J.W. Stevenson, J. Power Sources 115 (2003) 274.
[14] Y.-S. Chou, J.W. Stevenson, J. Power Sources 140 (2005) 340.
[15] B. Rauch, C. Compson, M. Liu, Hermetically sealed solid oxide fuel cells without sealant, submitted for publication (Applied for May 2004; provisional filing November 2005).
[16] R. Mistler, E. Twiname, Tape Casting Theory and Practice, American Ceramic Society, Westerville, OH, 2000.
[17] C. Compson, M. Liu, Impedance Spectroscopy Characterization of Hermetically Sealed SOFCs, in: P. Arora et al. (Eds.), Membranes and separators for fuel cells, Electrochemistry Society Proceedings PV 2004-XX, The Electrochemical Society, Penningtion, NJ, 2004, in press.